Robotica: (2020) volume 38, pp. 732–746. © Cambridge University Press 2019
doi:10.1017/S0263574719001012

Trunk-like Soft Actuator: Design, Modeling, and Experiments

Guanjun Bao*, Lingfeng Chen, Yaqi Zhang, Shibo Cai, Fang Xu, Qinghua Yang, and Libin Zhang

College of Mechanical Engineering, Zhejiang University of Technology, Hangzhou 310014, China. E-mails: 1160892244@qq.com, 554941660@qq.com, ccc@zjut.edu.cn, fangx@zjut.edu.cn, king@zjut.edu.cn, robot@zjut.edu.cn

(Accepted May 29, 2019. First published online: July 11, 2019)

SUMMARY
In recent years, soft robotics is widely considered as the most promising field for both research and application. First of all, the actuator is fundamental for designing, modeling, and controlling of soft robots. This paper presents a new type of pneumatic trunk-like soft actuator, which contains a chamber for stiffness adjustment in addition to three chambers for driving. Thus, the salient feature of the proposed actuator is the ability of stiffness self-regulation. The structure of the proposed actuator is described in detail. Then the theoretical models for elongation and bending motion of the actuator are established. The elongation as well as single-chamber and multi-chamber driving bending of the actuator were tested to verify the mathematical models. Finally, a dual-segment soft robot based on the proposed trunk-like soft actuator was developed and tested by experiments, which implies its potential application in practice.

KEYWORDS: Pneumatic soft actuator; Variable stiffness; Mathematic modeling.

1. Introduction

Nowadays, in addition to traditional industrial applications, robots are expected to do more work in other areas, such as medicine, rehabilitation, exploration, rescue, agriculture, and service. Instead of high precision and operation speed, flexibility, safety, environmental adaptability, and compliance are urgently required in these new practice fields. However, it raises great challenges for conventional robots using rigid mechanical structures to accomplish such tasks like earthquake rescue, military investigation, manipulating fragile items, and so on. By contrast, soft robots composed of soft materials have the abilities of deforming their shape, grasping fragile objects without causing damage, adapting to the surroundings, and operating in an unstructured environment. They can take the advantages of flexibility and adaptability to easily accomplish complex motions and tasks even without sensor and controller.

One of the most widely adopted forms for soft robotic driving is pneumatics. Various cavity prismatic bar structures made of silica gel, PVC, ECOFLEX, and other soft materials are the driving units for pneumatic soft robots. A variety of individual soft robotic fingers or arms composed of pneumatic soft driving units can achieve envelop grasping of target object, as shown in Fig. 1. In addition to grasping, several soft multi-fingered grippers/dual-arm grippers shown in Fig. 2 can also operate and control the target objects with certain flexibility. The research trend in recent years is multi-fingered robotic hand which imitates the structure of human hand and tries to achieve the function of perception and flexible manipulation, as shown in Fig. 3.

* Corresponding author. E-mail: gjbao@zjut.edu.cn

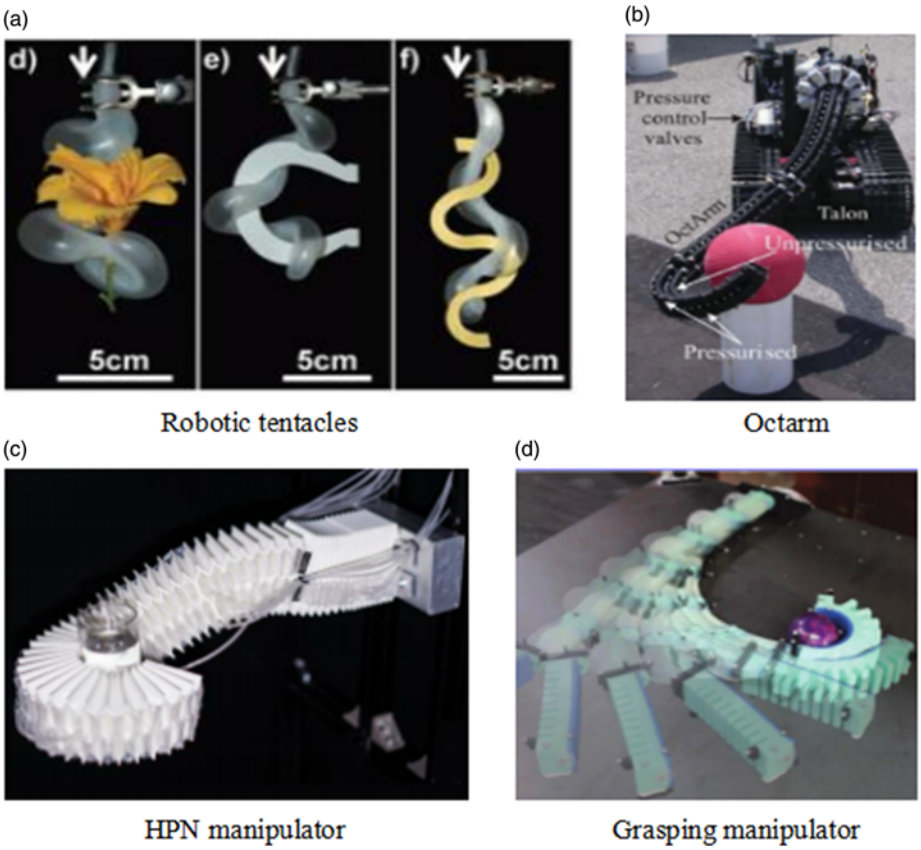

Fig. 1. Soft fingers.

The pneumatic driving units of prismatic soft actuators mentioned above can achieve complex movements, whose structures are mainly divided into the following four categories. (1) Single-chamber structure. It is able to achieve one-way bending by asymmetrical design of the air chamber, such as constrained cable,[1] unilateral thick wall,[2,3] and so on. The cross section of the air chamber can be designed in different geometric shapes of rectangular, circular, and hemi-circular. (2) Double-chamber structure. It is designed to realize bilateral bending in one plane by using integrated double-chamber structure[4] or separated double-chamber structure.[5,6] (3) Triple-chamber structure. Three-dimensional bending, elongation, and yaw can be realized by using integrated triple-chamber structure[7,8] or separated triple-chamber structure.[9] For instance, the flexible micro-actuator developed by Toshiba Corporation has three DOF (Degree of Freedom): stretching, bending, and twisting.[10] Also, the robotic tentacle developed by Ramses V. Martinez based on elastomer material can achieve complex three-dimensional motion and capture complicated objects.[11] (4) Multi-chamber/segment structure. Using grouped chamber array to compose pneumatic driving structure can achieve a large deformation and high output force for soft robots by deformation accumulation of each chambers.[12–14]

The aforementioned soft actuators can realize various forms of driving. However, they do not have the ability of stiffness regulation of themselves. Self-control of stiffness is an important function for octopus tentacles, trunks, and other soft biological structures to manipulate objects. Scientists and engineers also understand the significance of stiffness tunability for bioinspired soft robots. Researchers defined the stiffness for pneumatic artificial muscle according to the movement and mechanical property of the robots[15,16] and investigated the issue of stiffness control.[17] Some researchers claimed that the trunk robots and Oct-arm robots they developed had the characteristic of variable stiffness.[18–20] In fact, the referred robots were made of soft materials and they are compliant in nature even without driving. When driven by motor-cable or high-pressure fluid, the robots will become strong and rigid, which implies the increase of stiffness. However, the variability of their stiffness was accompanied by the motion process and coupled with the motion-driving

https://doi.org/10.1017/S0263574719001012 Published online by Cambridge University Press

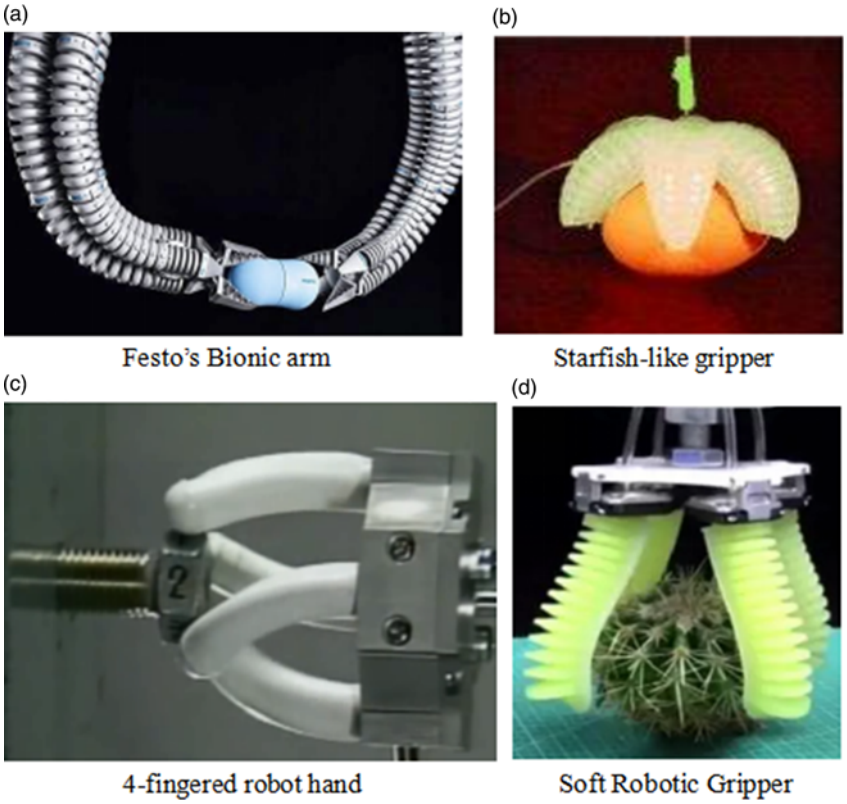

Fig. 2. Soft multi-fingered grippers.

Fig. 3. Soft robotic hands.

https://doi.org/10.1017/S0263574719001012 Published online by Cambridge University Press

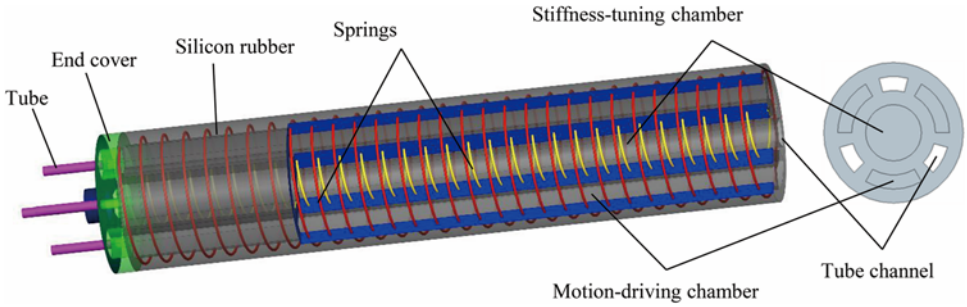

Fig. 4. Structure of trunk-like soft actuator.

parameters. These structures failed to achieve independent and active control of stiffness. Using granular material in the soft structure can achieve controllable stiffness with regulated negative pressure,[21] which was named as jamming.[22] The stiffness tunability relied on the friction among the granular material under negative pressure, which can hardly ensure continuous stiffness regulation[23] and repeatable performance.[24]

This paper proposed a new type of flexible pneumatic actuator named trunk-like soft actuator, which had three uniformly distributed motion-driving air chambers and one stiffness-regulating air chamber at the central axis. Composed of soft material and driven by compressed air, the actuator is capable of elongation, bending, and yaw. In addition, it is able to adjust its own stiffness dynamically during the process of operating target objects. In order to effectively achieve the motion and the stiffness controlling, this paper established the elongation and bending models of the actuator, built the testbed, and verified the theoretical models by experiments. Finally, we demonstrated the motion ability of a dual-segment soft robot which was designed based on the actuator.

2. Structure and Working Principle

The excellent flexibility and self-controllable stiffness of trunks and octopus arms are mainly due to their unique muscle tissue: muscular hydrostat, whose stiffness can be regulated by the fluid pressure inside their cavity. Inspired by this biological structure, we proposed a new type of pneumatic actuator, trunk-like soft actuator, which not only has the functions and features of conventional pneumatic soft actuators, but also can adjust its stiffness actively by controlling the air pressure of the central chamber. The mechanical scheme is shown in Fig. 4.

As discussed before, the triple-chamber structure of soft actuators always has integrated triple-chamber structure or separated triple-chamber structure, such as the flexible micro-actuator,[10] pneumatic spherical joint,[1] and soft gripper,[9] while we proposed a new structure with four chambers, which is the outstanding difference with existing system and ensures the variable stiffness. The trunk-like soft actuator is a cylinder with two kinds of chambers inside, that is, motion-driving chamber and stiffness-tuning chamber. The stiffness-tuning chamber locates at the central axis of the actuator, and the three motion-driving chambers are evenly distributed around the former. The motion-driving chambers are parallel with each other so that the actuator can realize different forms of motion, such as elongation, bending, and yaw in different directions and angles, just by adjusting the air pressures inside the three chambers. The stiffness-tuning chamber is cylindrical. When it is inflated with compressed air, the stiffness of trunk-like soft actuator will be improved. Thus the dynamic and independent adjustment of its stiffness is achieved.

The elastic extension rate of natural rubber can easily reach 1000% under external load. So the actuator made of natural rubber will expand easily, and its extended body can be times in length of the original structure when inflated with high-pressure air. Excessive expansion is not beneficial for the soft actuator to grasp the target object. Therefore, researchers adopted the methods of covering fiber[25,26] or fiber thread[27,28] on the surface of the rubber to restrain radial expansion of the actuator. It is quite easy in fabrication process to add reinforcement matter on the surface of soft material, while the integration between them is lower than that with internal embedded reinforcement structure. So spring is embedded in the shell of the proposed soft actuator, which can well inhibit the radial expansion. Furthermore, the restriction of radial expansion also contributes to axial stretching.

https://doi.org/10.1017/S0263574719001012 Published online by Cambridge University Press

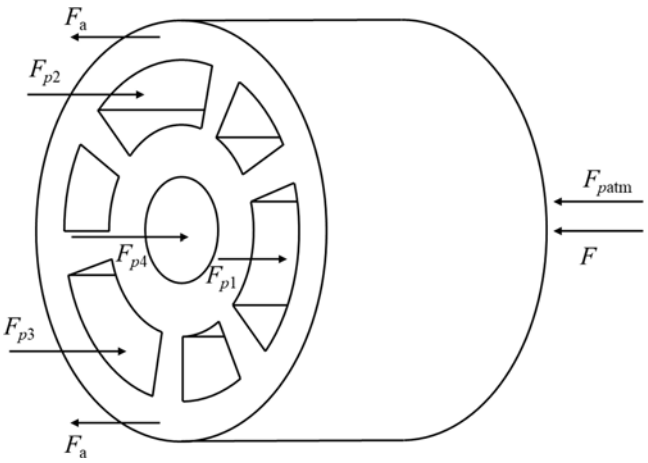

Fig. 5. Static analysis of the free end of trunk-like soft actuator.

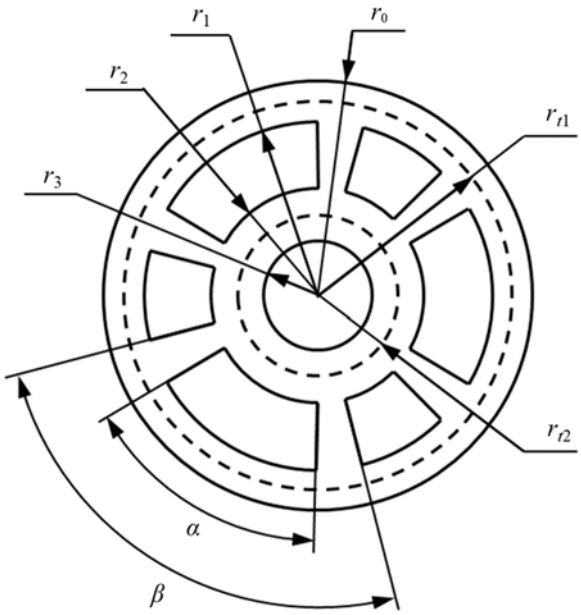

Fig. 6. Cross-section scheme of trunk-like soft actuator.

3. Modeling

3.1. Elongation

Static analysis of the free end of trunk-like soft actuator is shown in Fig. 5. The force equilibrium can be written as:

$$F = \sum_{i=1}^{4} F_{p_i} - F_a - F_{p_{\text{atm}}} \tag{1}$$

where F is the external force, namely the output force of trunk-like soft actuator, F_{pi} is the force generated by pressurized air inside the chamber, p_i is the air pressure inside chamber, $i = 1, 2, 3, 4$, F_a is the elastic force generated by silicone rubber, and $F_{p_{\text{atm}}}$ is the atmospheric pressure.

As shown in Fig. 6, the parameters in the trunk-like soft actuator cross section are defined as follows: r_0 is the outer radius of the actuator, r_1 is the outer radius of motion-driving chamber, r_2 is the inner radius of motion-driving chamber, r_3 is the radius of stiffness-tuning chamber, r_{t1} is the radius of outer spring, r_{t2} is the radius of inner spring, α is the inner wall central angle of motion-driving chamber, and β is the outer wall central angle of motion-driving chamber.

https://doi.org/10.1017/S0263574719001012 Published online by Cambridge University Press

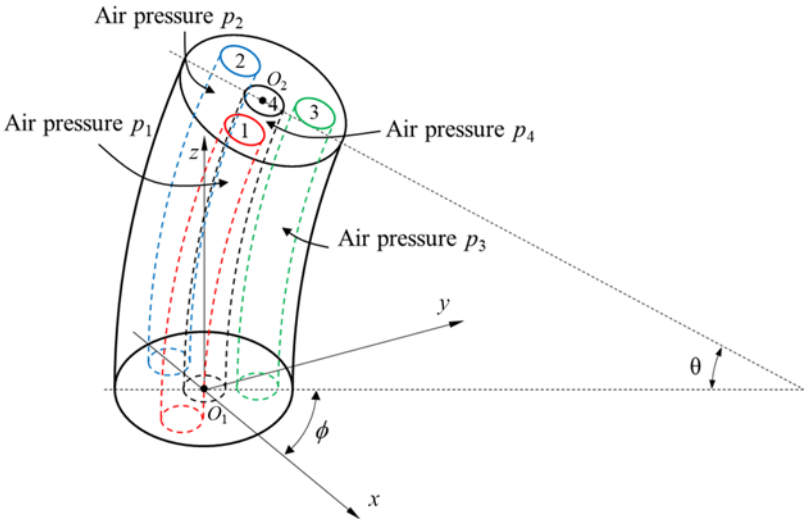

Fig. 7. Bending state of trunk-like soft actuator.

There are totally four chambers in the trunk-like soft actuator, including three motion-driving chambers and one stiffness-tuning chamber. When the four chambers are inflated with isobaric pressurized air at the same time, the actuator will elongate axially. According to the force and geometric analysis, we can get the static model of the trunk-like soft actuator as:

$$F = \left[\frac{3}{2}\alpha(r_1^2 - r_2^2) + \pi r_3^2\right](p - p_{\text{atm}}) - E\left[\pi\left(r_0^2 - r_3^2\right) - \frac{2\pi - 3\beta + 3\alpha}{2}\left(r_1^2 - r_2^2\right)\right]\frac{\Delta L}{L_0} \tag{2}$$

When external force $F = 0$, the expression of elongation ΔL can be obtained as:

$$\Delta L = \frac{\left[3\alpha\left(r_1^2 - r_2^2\right) + 2\pi r_3^2\right](p - p_{\text{atm}})\,L_0}{E\left[2\pi\left(r_0^2 - r_3^2\right) - (2\pi - 3\beta + 3\alpha)\left(r_1^2 - r_2^2\right)\right]} \tag{3}$$

3.2. Bending

The constant curvature model provides a widely accepted mean to determine the pose of continuum robot as well as soft robot,[29] which was employed here for the geometrical analysis. When the air pressures p_i in the chambers are not equal, the trunk-like soft actuator will bend, as shown in Fig. 7, where ϑ is the bending angle (which is the central angle of the arc formed by the bended actuator) and ϕ is the angle which defines the yaw direction of the actuator in space. The rubber material can be taken as a set of parallel spring and damper, and its strain and stress are the sum of the two elements.[30–32] During the static modelling process, the damping effect of the rubber material can be ignored. Therefore, the four chambers can be simplified as four springs, and their positions are at the centroid of corresponding air chambers respectively, as shown in Fig. 8. The lengths of the springs were defined as l_1, l_2, l_3, and l_4 respectively, and the initial length of trunk-like soft actuator was defined as L_0. Because the motion-driving chambers are symmetrically and evenly distributed around the axis of the actuator, the position of the springs corresponding to motion-driving chambers is on the same circle whose radius was defined as r. A differential segment of the trunk-like soft actuator was shown in Fig. 9.

According to the geometric scheme in Fig. 9, we can get:

$$\phi = \tan^{-1}\frac{\sqrt{3}\,(l_3 - l_2)}{l_2 + l_3 - 2l_1} \tag{4}$$

$$\theta = \frac{\sqrt{2\left[(l_1 - l_2)^2 + (l_2 - l_3)^2 + (l_3 - l_1)^2\right]}}{3r} \tag{5}$$

https://doi.org/10.1017/S0263574719001012 Published online by Cambridge University Press

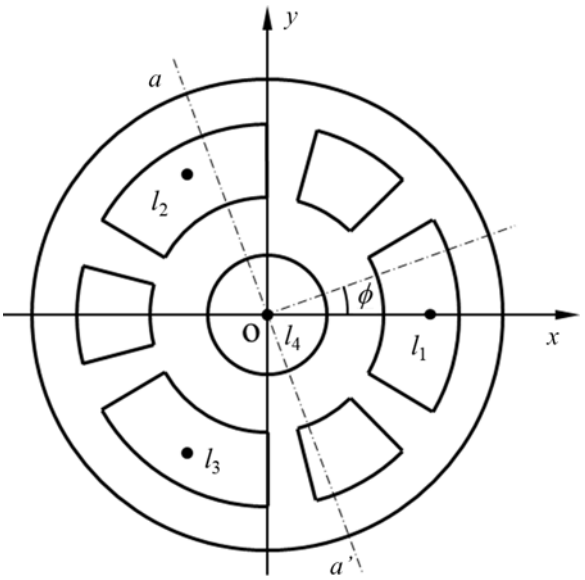

Fig. 8. Simplification of trunk-like soft actuator.

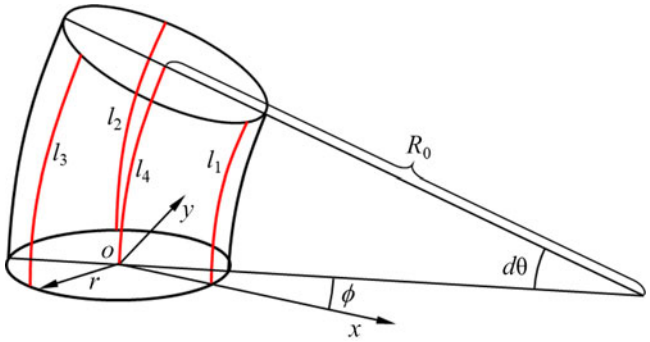

Fig. 9. A differential segment of trunk-like soft actuator.

$$R_0 = \frac{(l_1 + l_2 + l_3)\, r}{\sqrt{2\left[(l_1 - l_2)^2 + (l_2 - l_3)^2 + (l_3 - l_1)^2\right]}} \tag{6}$$

where R_0 is the radius of curvature of the bending trunk-like soft actuator.

The key to establish the bending model for the actuator is to solve the force/moment balance equation of the free end. The mechanic diagram at the free end was shown in Fig. 10. From Eq. (1), when external force $F = 0$, the force balance equation can be rewritten as:

$$\sum_{i=1}^{4} F_{p_i} = F_a + F_{p_{\text{atm}}} \tag{7}$$

Substituting Eqs. (4)–(6) into Eq. (7), we can get:

$$\phi = \tan^{-1} \frac{\sqrt{3}\,(\Delta p_3 - \Delta p_2)}{\Delta p_2 + \Delta p_3 - 2\Delta p_1} \tag{8}$$

$$\theta = \frac{4L_0\left(r_1^3 - r_2^3\right)\sin\frac{\alpha}{2}\sqrt{2\left[(\Delta p_1 - \Delta p_2)^2 + (\Delta p_2 - \Delta p_3)^2 + (\Delta p_3 - \Delta p_1)^2\right]}}{3E\left[\pi\left(r_0^4 - r_3^4\right) - \frac{2\pi - 3\beta + 3\alpha}{2}\left(r_1^4 - r_2^4\right)\right]} \tag{9}$$

https://doi.org/10.1017/S0263574719001012 Published online by Cambridge University Press

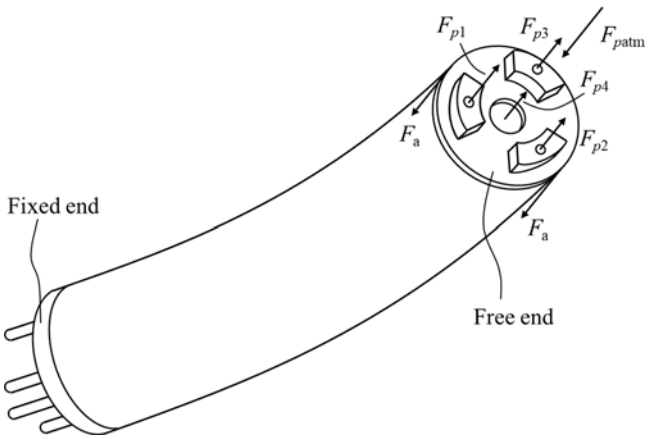

Fig. 10. Mechanical analysis for the free end of trunk-like soft actuator.

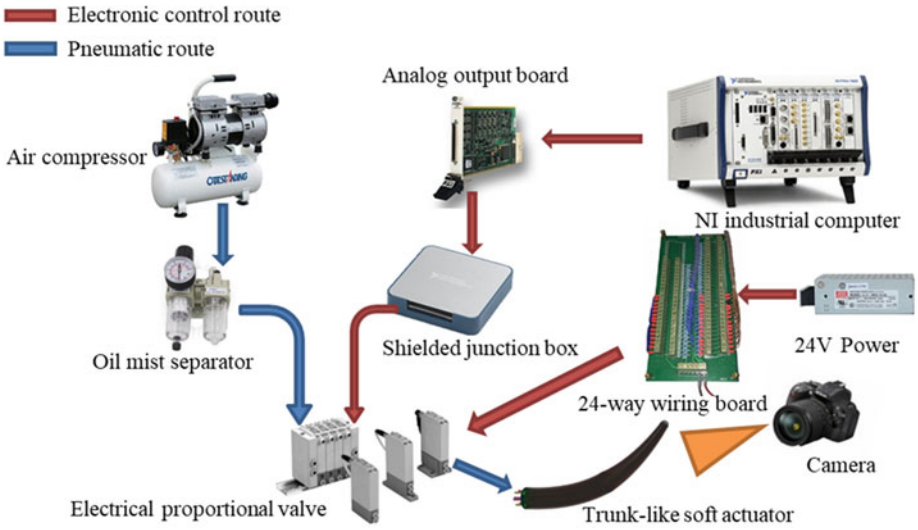

Fig. 11. Principle of experimental system.

$$R_0 = \frac{3E\left[\pi\left(r_0^4 - r_3^4\right) - \frac{2\pi-3\beta+3\alpha}{2}\left(r_1^4 - r_2^4\right)\right] + 4\left(r_1^3 - r_2^3\right)\sin\frac{\alpha}{2}\left(\Delta p_1 + \Delta p_2 + \Delta p_3\right) r}{4\left(r_1^3 - r_2^3\right)\sin\frac{\alpha}{2}\sqrt{2\left[\left(\Delta p_1 - \Delta p_2\right)^2 + \left(\Delta p_2 - \Delta p_3\right)^2 + \left(\Delta p_3 - \Delta p_1\right)^2\right]}} \tag{10}$$

where Δp_i (i = 1, 2, 3) is the pressure difference between chamber i and the atmosphere.

4. Validation Experiments

4.1. Experimental testbed

The experimental scheme for trunk-like soft actuator is shown in Fig. 11, including electronic control route and pneumatic route.

A National Instruments (NI) industrial computer with Labview program was used for analog signal output to the electrical proportional valve. Since the electrical proportional valves need 24 V power supply and a reference voltage for the input voltage signal, a 24-way wiring board was added to simplify the circuit. The industrial computer is NI PXI-1042Q with eight expansion slots, and the controller is NI PXI-8105 based on the Intel Core Duo processor T2500. We chose NI PXI-6704 as the analog output card. This module can provide 16-channel voltage output in the range of -10 V to 10 V and 16-channel direct current output in the range of 0 mA to 10 mA as well as 8-channel digital

https://doi.org/10.1017/S0263574719001012 Published online by Cambridge University Press

Table I. Structural parameters of the trunk-like soft actuator.

Parameter	**Symbol**	**Unit**	**Value**
Initial length of the actuator	L_0	mm	123.5
Elastic modulus	E	MPa	0.249
Shore A hardness	HA	deg	35
Outer radius of the actuator	r_0	mm	16
Outer radius of motion-driving chamber	r_1	mm	13
Inner radius of motion-driving chamber	r_2	mm	8
Radius of stiffness-tuning chamber	r_3	mm	4
First arc angle	α	rad	$\pi/3$
Second arc angle	β	rad	$\pi/2$
Atmospheric pressure	p_{atm}	MPa	0.1

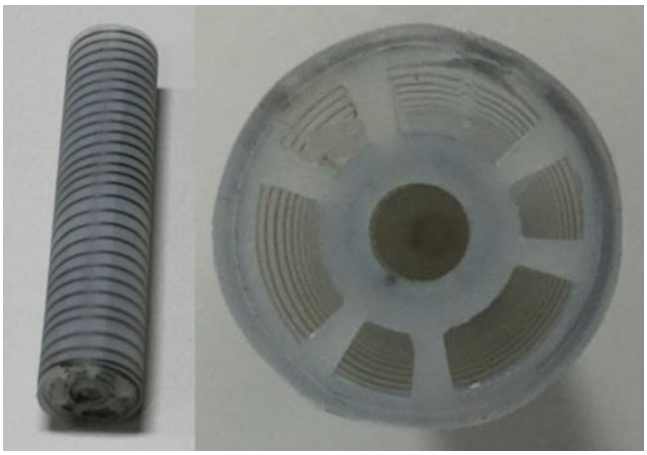

Fig. 12. Prototype of trunk-like soft actuator.

I/O. The shielded junction box is NI SCB-68A which is a plug-in DAQ (Data Acquisition) device with 68-pin connection port.

Air compressor was adopted as the pneumatic source. The pressurized air for experiments was finally obtained by the process of oil mist separator and pressure regulating valve. The compressed air was inflated into the chambers of trunk-like soft actuator via electrical proportional valves. The electrical proportional valve can regulate its output air pressure according to the voltage signal from the electronic control route. The electrical proportional valve is SMC ITV0050-3BS, whose input control signal ranges from 0 V to 5 V, and output pressure ranges from 0.001 MPa to 0.9 MPa with linearity of $\pm 1\%$.

The prototype of trunk-like soft actuator is shown in Fig. 12, which was made of natural rubber NR-SVR3L with Shore hardness of A35. The mechanical parameters of the trunk-like soft actuator are listed in Table I. The experiment platform is shown in Fig. 13.

4.2. Tensile test of silicone rubber

Tensile test of silicone rubber was carried out to determine the elastic modulus of silicone rubber. We used INSTRON 5966 Dual Column Testing System as the tensile test platform. And the rubber samples for tensile test were made in standard mold, whose width is 5.10 mm, thickness is 1.00 mm, and effective length is 20.00 mm.

We set the stretching rate as 200 mm/min according to the properties of rubber material. Five repeated experiments were carried out, and the obtained results are shown in Fig. 14. It can be clearly seen that the stress was almost linear with the strain in the elastic deformation stage and the samples broke when elongation percentage reached about 1200%. We calculated the elastic modulus of each sample according to the test data and get final elastic modulus of rubber as 0.995 MPa by averaging all the elastic modulus of each sample, as shown in Table II.

https://doi.org/10.1017/S0263574719001012 Published online by Cambridge University Press

Table II. Tensile test data.

Sample	Tensile strength (MPa)	Breaking elongation (%)	Elastic modulus (MPa)
Sample 1	9.584	1036	1.000
Sample 2	8.364	1191.7	0.873
Sample 3	10.680	1223.7	0.987
Sample 4	16.256	1537.9	1.131
Sample 5	11.648	1390.3	0.981
Average	7.121	1275.9	0.995
Standard deviation	3.077	172.69	0.082

Note: The tensile strength is the maximum tensile stress during the tensile test. The breaking elongation is the strain at the moment of maximum tensile stress. The elastic modulus is the ratio of tensile strength to elongation percentage.

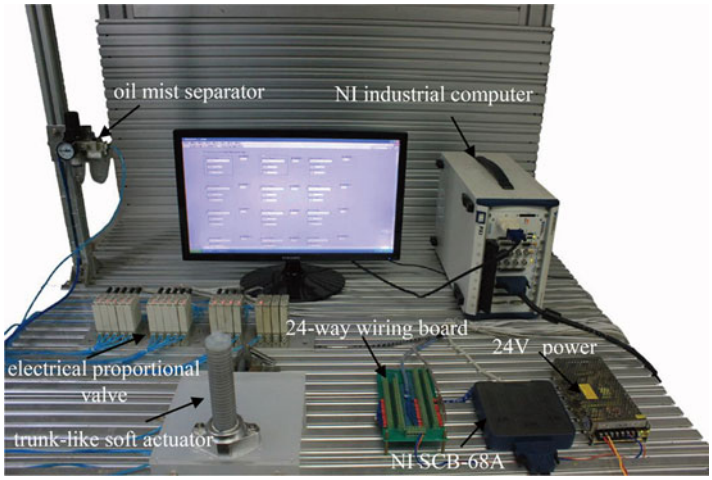

Fig. 13. Experimental platform.

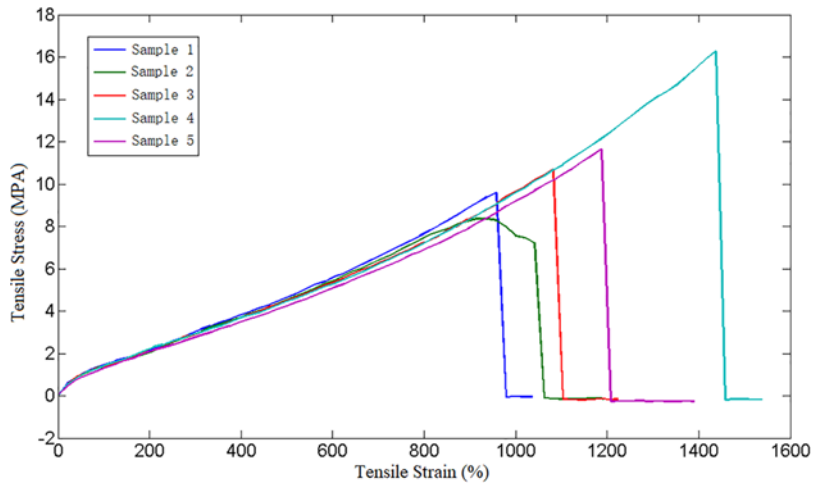

Fig. 14. Curves of tensile test.

4.3. Elongation experiment

Inflation and deflation experiments for the trunk-like soft actuator were carried out without external load. In the elongation experiment, the four chambers of trunk-like soft actuator were inflated with equal pressurized air. We conducted four repeated inflation and deflation experiments, and recorded the pressure and the length of the actuator at each increment of 0.009 MPa. The relationship between

https://doi.org/10.1017/S0263574719001012 Published online by Cambridge University Press

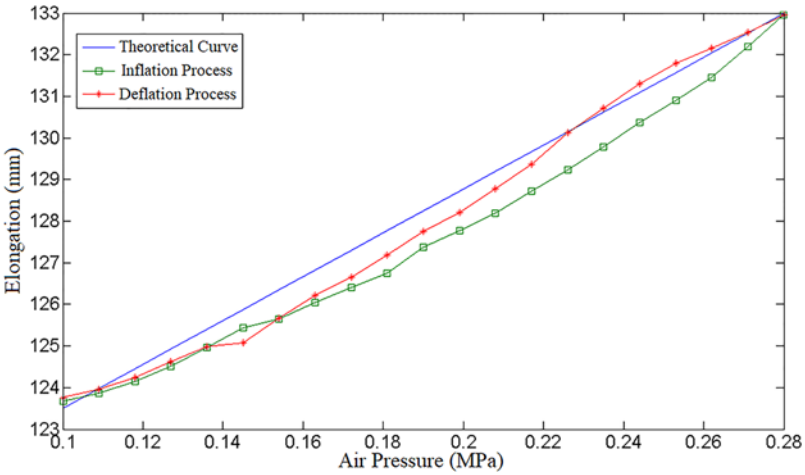

Fig. 15. Comparison between experimental data and simulation results.

the extended length and the air pressure could be derived according to the data from inflation process as well as deflation process.

Based on the parameters of trunk-like soft actuator and the elastic modulus of the rubber obtained in the tensile test, we can get the simulation results of the elongation according to the mathematic model. The comparison between experimental data and simulation results is shown in Fig. 15. (The initial length of the actuator is 150 mm; however, because of the holder, the effective length is only 123.5 mm.)

It can be seen from Fig. 15 that the experimental curve is a little lower than that of the theoretical simulation. The reason relies on the embedded springs inside the trunk-like actuator, which actually to some extent hindered the elongation of the actuator. However, since the spring wire is thin, the effect of the springs on elongation was ignored in the theoretical model.

4.4. Single-chamber driving bending experiment

In the single-chamber driving bending experiment, only one motion-driving chamber was inflated, and the others maintained atmospheric pressure. The air pressure was controlled by voltage signal via electrical proportional valve. The pressure range for inflation experiment was 0–0.252 MPa with an increment of 0.018 MPa. We recorded experimental process by taking photos, making sure that lens was perpendicular to the bending plane of the actuator. Thus, the bending angle of the actuator could be measured in the photos. The bending process of the actuator is shown in Fig. 16 (selected eight shots). Simulation results of single-chamber driving bending process can be obtained according to the bending model. The comparison between experimental data and simulation results is shown in Fig. 17.

It can be seen from Fig. 17 that when the pressure was in the range of 0.0 MPa to 0.2 MPa, the experimental results were in good agreement with the simulation curve. However, when the pressure exceeded 0.2 MPa, the experimental data deviated from the simulation results and the bending angle were not linear with the pressure anymore. When the pressure in the chamber is high enough, the wall of the actuator will partially bulge, although there is constraint of springs in the wall. And the partial bulge will cause the wall of the air chamber to become thinner, which further weakens the resistance to expansion. Thus it is easy to blister at the weakness point of the wall under high pressure, which results in a sharp increase in bending angle. Therefore, when the pressure exceeded 0.2 MPa, the actual bending angle was much larger than theoretical result, and the curve was parabolic, as shown in Fig. 17.

The sharp change of the bending angle is nonstationary work stage, which is not allowed in practice. If bigger bending angle is required, it can be realized by enhancing the thickness of the wall of the actuator, reducing the stiffness of the embedded spring, or using harder rubber materials.

https://doi.org/10.1017/S0263574719001012 Published online by Cambridge University Press

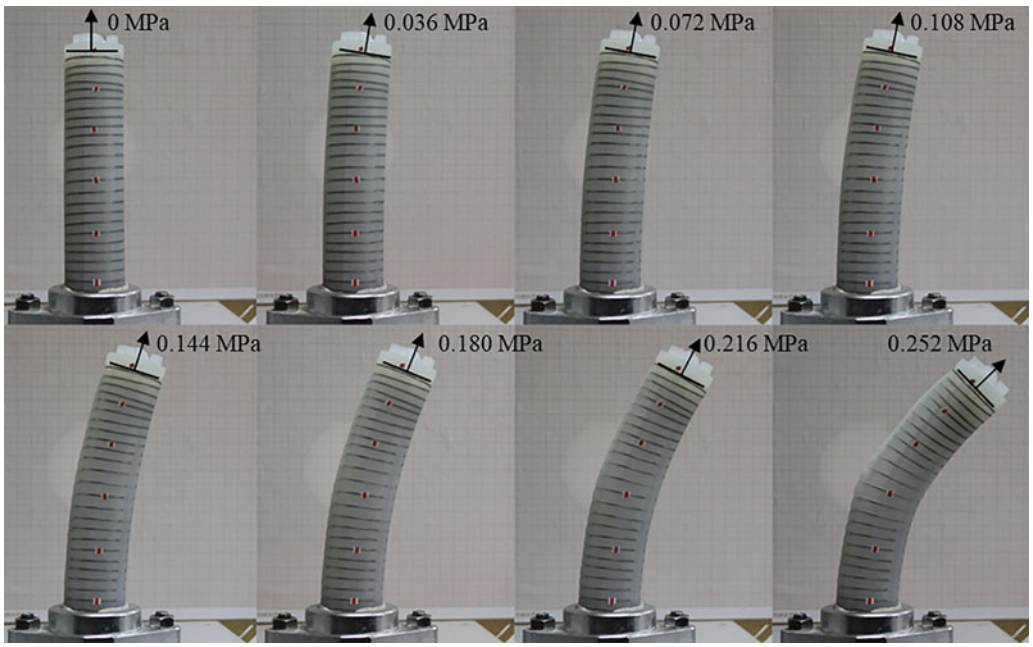

Fig. 16. Single-chamber driving bending experiment.

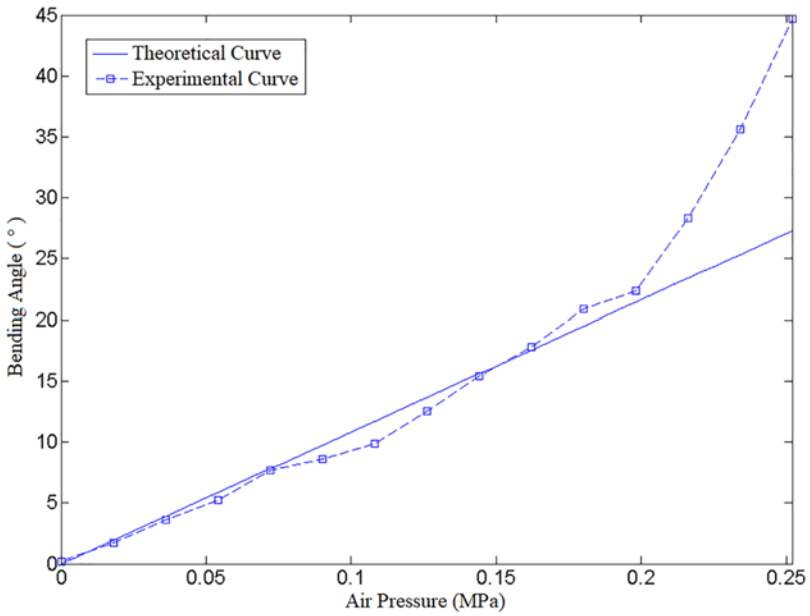

Fig. 17. Comparison between experimental data and simulation results.

4.5. Multi-chamber driving bending experiment

Multi-chamber driving bending experiment demonstrated the ability of curving in any direction. In this experiment, three motion-driving chambers were filled with high-pressure air of different pressures. The results of the experiment are shown in Fig. 18. The numbers 1, 2, and 3 indicate the three motion-driving chambers of the actuator, and the values after the number indicate the corresponding voltage signals of each chamber. The experimental results showed that the trunk-like soft actuator can be driven to bend in all directions by appropriately controlling the combination of the air pressures inside the three motion-driving chambers.

https://doi.org/10.1017/S0263574719001012 Published online by Cambridge University Press

Fig. 18. Multi-chamber driving bending experiment.

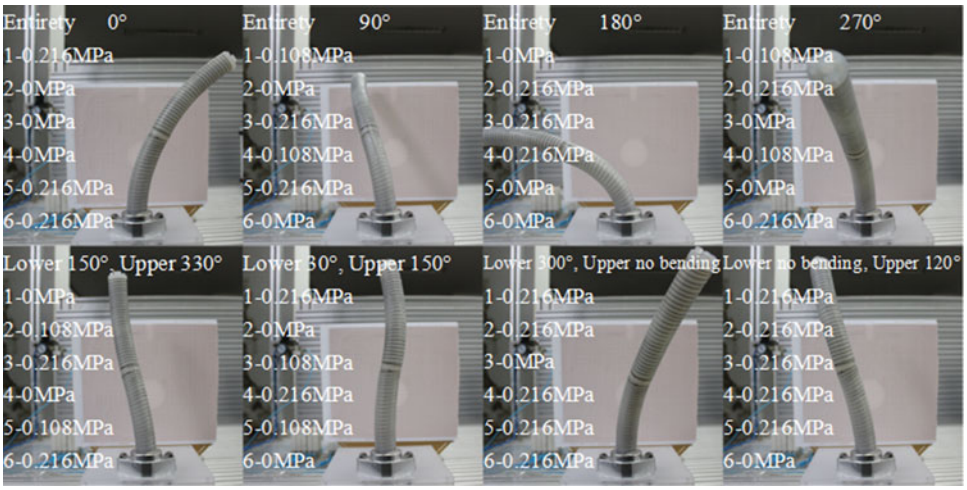

Fig. 19. Dual-segment soft robot experiments ("entirely," "upper," and "lower" indicate respectively the bending direction of the whole soft robot, the upper segment, and the lower segment, 1–3 indicate the lower motion-driving chambers, 4–6 indicate the upper motion-driving chambers, and the value after the number indicates the air pressure).

4.6. Dual-segment soft robot

We designed a dual-segment robot by assembling two trunk-like soft actuators in series. Experiments were carried out to demonstrate its motion ability. We conducted eight experiments with different combinations of air pressures, and the gestures were also recorded by camera. The experimental parameters and the corresponding experimental results were shown in Fig. 19, where "entirety" indicates the bending direction of the whole dual-segment soft robot, "upper" indicates the bending direction of the upper segment, "lower" indicates the bending direction of the lower segment, numbers 1–6 indicate the six motion-driving chambers, and the value after the number indicates the air pressure.

5. Conclusions

This paper presented a new type of pneumatic actuator, trunk-like soft actuator, which has a cylinder body with a stiffness-tuning chamber at the central axis and three motion-driving chambers evenly

https://doi.org/10.1017/S0263574719001012 Published online by Cambridge University Press

distributed around the former. Due to this specially designed structure, the actuator has the capability of elongation, three-dimensional bending, and dynamic self-control of stiffness. The trunk-like soft actuator was made of natural rubber, which ensures its flexibility and compliance. Besides, the actuator was embedded with springs in the shell to limit the radial expansion, which improves the predictability and controllability.

The elongation and bending models were established to predict the motion, position, and gesture of the soft actuator, which provides theoretical basis for potential applications. We tested and verified the elongation as well as single-chamber and multi-chamber driving bending of the actuator. The comparison between the experimental data and the theoretical simulation results implied that the actual elongation was slightly smaller than the theoretical value at the same pressure. This small error was caused by the springs embedded in the shell. In single-chamber driving bending experiment, when the air pressure was 0.0–0.2 MPa, the experimental data and theoretical simulation results agreed with each other very well, which verified the mathematic model. And the multi-chamber bending experiment showed that the trunk-like soft actuator has the capability of three-dimensional bending.

Besides, we designed a dual-segment soft robot based on the proposed trunk-like soft actuator and realized its bending motion in any direction, which showed that the trunk-like soft actuator has large potential for applications, such as endoscope robot, rescue robot for mining accident or earth quake, and end-effector for manipulation. The theoretical models will contribute to the design and control of the soft robots that are based on the actuator.

Although soft robots have dominant advantages over their traditional rigid counterparts, they do challenge the scientist and engineers a lot in quite several aspects. In the case of this research, there are still limitations to be solved before the actuator can be used in practice. The delicate structure ensures the ability of self-stiffness tuning, while resulting in difficulty of parameters optimization and complex fabrication. Furthermore, the complicated design causes the sophisticated mathematical model as demonstrated in this paper. Moreover, the sensing and controlling in practice are also difficult problems. All these limitations will be considered and investigated in the future work.

Acknowledgments

This research was financially supported by the National Science Foundation of China (Grant number: 51775499, 51605434) and NSFC-Zhejiang Joint Fund for the Integration of Industrialization and Informatization (Grant number: U1509212).

6. Author Disclosure Statement

The authors declare that no competing financial interests exist.

References

1. B. Guanjun, Y. Pengfei, X. Zonggui, L. Kun, Z. Libin and Y. Qinghua, "Pneumatic bio-soft robot module: Structure, elongation and experiment," *Int. J. Agric. Biol. Eng.* **10**(2), 114–122 (2017).
2. B. Gorissen, R. Donose, D. Reynaerts and M. D. Volder, "Flexible pneumatic micro-actuators: Analysis and production," *Procedia Eng.* **25**, 681–684 (2011).
3. D. P. Holland, C. Abah, M. Velasco-Enriquez, M. Herman, G. J. Bennett and E. A. Vela, "The Soft Robotics Toolkit: Strategies for overcoming obstacles to the wide dissemination of soft-robotic hardware," *IEEE Robot. Autom. Mag.* **24**(1), 57–64 (2017).
4. K. Suzumori, S. Endo, T. Kanda, N. Kato and H. Suzuki, "A Bending Pneumatic Rubber Actuator Realizing Soft-bodied Manta Swimming Robot," *IEEE International Conference on Robotics and Automation*, Rome, Italy (2007) pp. 4975–4980.
5. A. Al-Ibadi, S. Nefti-Meziani and S. Davis, "Valuable Experimental Model of Contraction Pneumatic Muscle Actuator," *21st International Conference on Methods and Models in Automation and Robotics (MMAR)*, Miedzyzdroje, Poland (2016).
6. B. Guanjun, S. Tiefeng, L. Shanghui, W. Zhiheng and Y. Qinghua, "Static model of flexible pneumatic swaying joint," *Trans. Chin. Soc. Agric. Mach.* **42**(6), 198–202 (2011).
7. K. Suzumori, S. Iikura and H. Tanaka, "Flexible Microactuator for Miniature Robots," *Proceedings of the IEEE Micro Electro Mechanical Systems Conference*, Nara, Japan (1991) pp. 204–209.
8. R. V. Martinez, J. L. Branch, C. R. Fish, L. Jin, R. F. Shepherd and R. M. D. Nunes, "Robotic tentacles with three-dimensional mobility based on flexible elastomers," *Adv. Mater.* **25**(2), 205–212 (2013).
9. L. A. T. Al Abeach, S. Nefti-Meziani and S. Davis, "Design of a variable stiffness soft dexterous gripper," *Soft Robot.* **4**(3), 274–284 (2017).

10. K. Suzumori, S. Iikura and H. Tanaka, "Development of Flexible Microactuator and its Applications to Robotic Mechanisms," *IEEE International Conference on Robotics and Automation*, Sacramento, California, vol. 2 (1991) pp. 1622–1627.
11. R. V. Martinez, C. R. Fish, X. Chen and G. M. Whitesides, "Elastomeric origami: Programmable paper-elastomer composites as pneumatic actuators," *Adv. Funct. Mater.* **22**(7), 1376–1384 (2012).
12. M. A. Robertson, H. Sadeghi, J. M. Florez and J. Paik, "Soft pneumatic actuator fascicles for high force and reliability," *Soft Robot.* **4**(1), 23–32 (2017).
13. H. Jiang, X. Liu, X. Chen, Z. Wang and Y. Jin, "Design and Simulation Analysis of a Soft Manipulator Based on Honeycomb Pneumatic Networks," *IEEE International Conference on Robotics and Biomimetics*, Qingdao, China (2017) pp. 350–356.
14. A. Jusufi, D. Vogt, R. Wood and G. Lauder, "Undulatory swimming performance and body stiffness modulation in a soft robotic fish-inspired physical model," *Soft Robot.* **4**(3), 202–210 (2017).
15. X. Fu, M. Fang and B. Li, "Theoretic analysis of stiffness characteristics of the pneumatic muscle actuator," *Mach. Tool Hydraul.* **35**(2), 109–111 (2007).
16. W. Binrui, Z. Weiyi and X. Hong, "Static actuating characteristics of intelligent pneumatic muscle," *Trans. Chin. Soc. Agric. Mach.* **40**(3), 208–212 (2009).
17. G. Tonietti and A. Bicchi, "Adaptive Simultaneous Position and Stiffness Control for a Soft Robot Arm," *Proceedings of the 2002 IEEE/RSJ International Conference on Intelligent Robots and Systems*, Lausanne, Switzerland (2002) pp. 1992–1997.
18. D. Held, Y. Yekutieli and T. Flash, "Characterizing the Stiffness of a Multi-Segment Flexible Arm During Motion," *Proceedings of IEEE International Conference on Robotics and Automation*, St. Paul, Minnesota, USA (2012) pp. 3825–3832.
19. A. Jiang, E. Secco, H. Wurdemann, T. Nanayakkara and K. Althoefer, "Stiffness-Controllable Octopus-like Robot Arm for Minimally Invasive Surgery," *3rd Joint Workshop on New Technologies for Computer/Robot Assisted Surgery*, Verona, Italy (2013).
20. C. Laschi, B. Mazzolai, V. Mattoli, M. Cianchetti and P. Dario, "Design of a biomimetic robotic octopus arm," *Bioinspir. Biomim.* **4**(1), 015006 (2009).
21. J. Fraś, J. Czarnowski, M. Maciaś, J. Główka, M. Cianchetti and A. Menciassi,"New STIFF-FLOP Module Construction Idea for Improved Actuation and Sensing," *IEEE International Conference on Robotics and Automation*, Seattle, WA, USA (2015) pp. 2901–2906.
22. E. Brown and D. Meiron, "Universal robotic gripper based on the jamming of granular material," *Proc. Natl. Acad. Sci. U. S. A.* **107**(44), 18809 (2010).
23. Y. Li, Y. Chen and Y. Wei, "Passive particle jamming and its stiffening of soft robotic grippers," *IEEE Trans. Robot.* **33**(2), 446–455 (2017).
24. J. Amend, N. Cheng, S. Fakhouri and B. Culley, "Soft robotics commercialization: Jamming grippers from research to product," *Soft Robot.* **3**(4), 213–222 (2016).
25. R. V. Martinez, J. L. Branch, C. R. Fish, L. Jin, R. F. Shepherd and R. M. D. Nunes, "Robotic tentacles with three-dimensional mobility based on flexible elastomers," *Adv. Mater.* **25**(2), 205–212 (2013).
26. D. G. Caldwell, G. A. Medrano-Cerda and M. J. Goodwin, "Braided Pneumatic Actuator Control of a Multi-Jointed Manipulator," *International Conference on Systems, Man and Cybernetics*, Le Touquet, France, vol. 1 (1993) pp. 423–428.
27. T. V. J. Tarvainen and W. Yu, "Preliminary Results on Multi-Pocket Pneumatic Elastomer Actuators for Human–Robot Interface in Hand Rehabilitation," *IEEE International Conference on Robotics and Biomimetics*, Zhuhai, China (2015) pp. 2635–2639.
28. R. Deimel and O. Brock, "A Compliant Hand Based on a Novel Pneumatic Actuator," *IEEE International Conference on Robotics and Automation*, Karlsruhe, Germany (2013) pp. 2047–2053.
29. R. J. Webster III and B. A. Jones, "Design and kinematic modeling of constant curvature continuum robots: A review," *Int. J. Robot. Res.* **29**(13), 1661–1683 (2010).
30. K. Nakajima, H. Hauser, R. Kang, E. Guglielmino, D. G. Caldwell and R. Pfeifer, "A soft body as a reservoir: case studies in a dynamic model of octopus-inspired soft robotic arm," *Front. Comput. Neurosci.* **7**(28), 91 (2013).
31. T. J. Zheng, D. T. Branson, E. Guglielmino, R. Kang and A. Gustavo, "Model validation of an octopus inspired continuum robotic arm for use in underwater environments," *J. Mech. Robot.* **5**(2), 021004 (2013).
32. R. Kang, D. T. Branson, T. J. Zheng, E. Guglielmino and D. G. Caldwell, "Design, modeling and control of a pneumatically actuated manipulator inspired by biological continuum structures," *Bioinspir. Biomim.* **8**(3), 036008 (2013).